Supporting Information

Competition between hydrogen and halogen bonding in the structures of 5,10-dihydroxy-5,10-dihydroboranthrenes

Krzysztof Durka,[a]* Sergiusz Luliński,[a] Katarzyna Jarzembska[b], Jaromir Smętek,[a] Janusz Serwatowski,[a] Krzysztof Woźniak[b]*

[a] Warsaw University of Technology, Faculty of Chemistry, Department of Physical Chemistry, Noakowskiego 3, 00-664, Warszawa, Poland

[b] University of Warsaw, Department of Chemistry, Structural Research Laboratory, Pasteura 1, 02-093, Warszawa, Poland

* Corresponding authors: Krzysztof Woźniak (kwozniak@chem.uw.edu.pl)
Krzysztof Durka (kdurka@gmail.com)

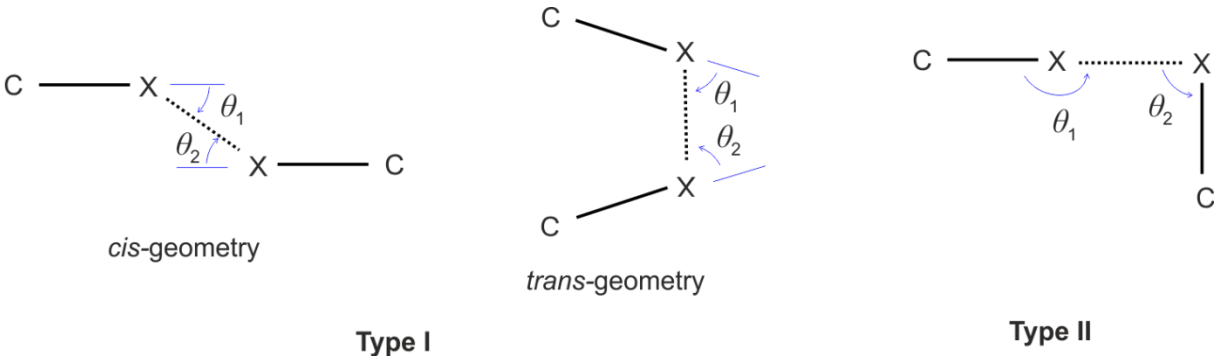

Scheme S1. Geometry classification of halogen-halogen interactions. Type I: both θ angles are equal. Type II: θ_1 is close to 180º and θ_2 to 90º.

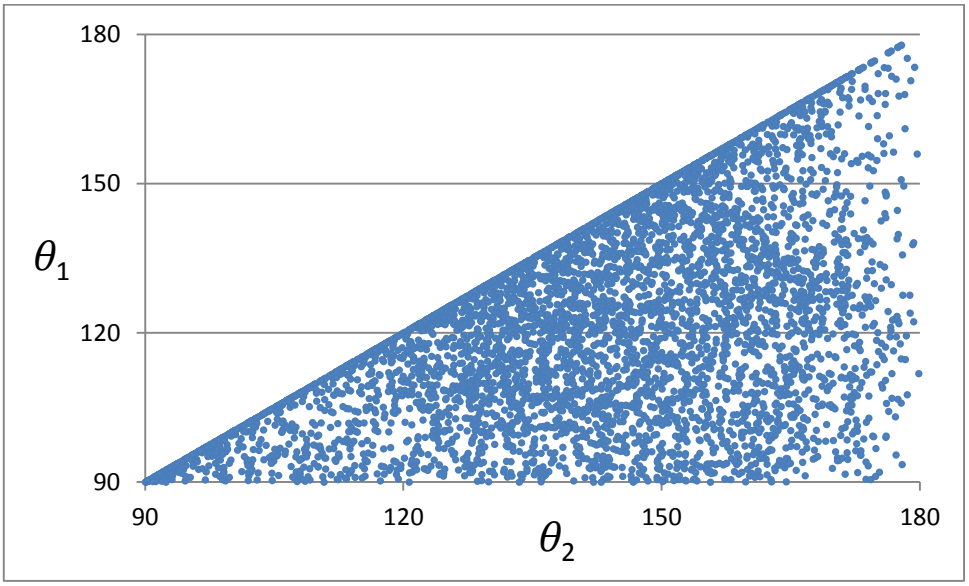

Figure S1. Diagram representing the distribution of θ_1 (C1–F1…F2) and θ_2 (C1–F1…F2) angles ($\theta_1 \leq \theta_2$) from the intermolecular C1–F1…F2–C2 contacts, shorter than the sum of the van der Waals radii ($d_{F\ldots F} < 2.95$ Å) in the Cambridge Structural Database (Allen, 2002).

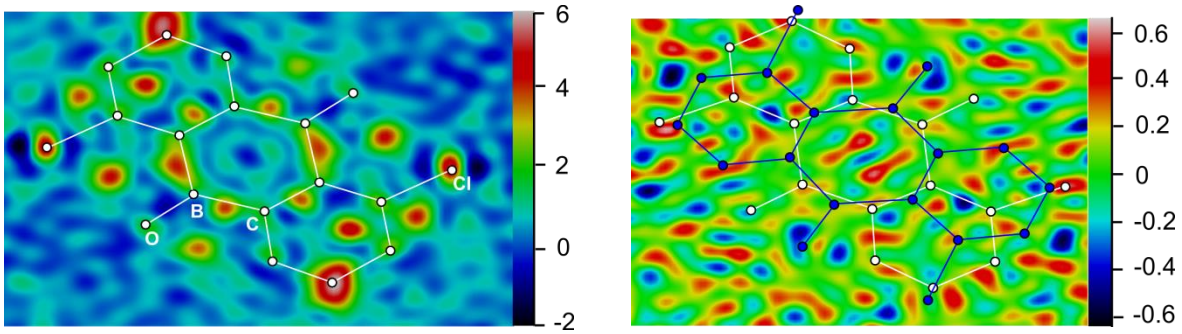

(*a*) (*b*)

Figure S2. Difference Fourier density maps for the structure of (III) with disorder (*a*) excluded, (*b*) included in the refinement. Color coding: white (III)-A, blue (III)-B. Maps were produced using the *MAPVIEW* program within *WinGX* (Farrugia, 1999).

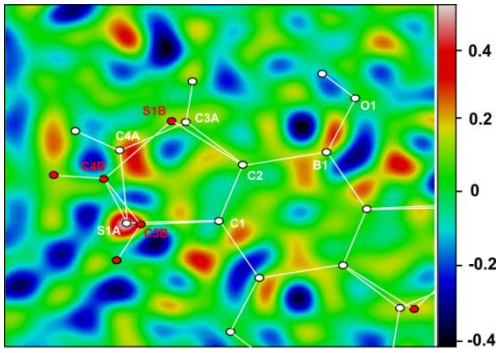

Figure S3. Difference Fourier density maps for the structure of (V) showing the disorder within the thiophene ring.

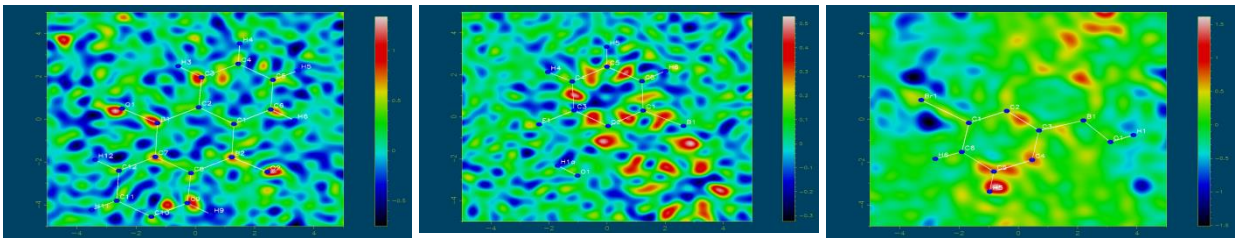

(*a*) (*b*) (*c*)

Figure S4. Difference Fourier density maps for the structures of *(a)* (I), *(b)* (II) and *(c)* (IV).

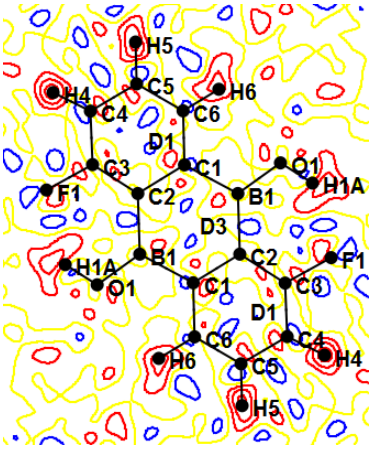

Figure S5. Residual electron density map for (II) after UBDB2011 parameters transfer (0.05 e·Å^{-3} contours; blue solid lines positive, red solid lines negative, yellow dashed lines zero).

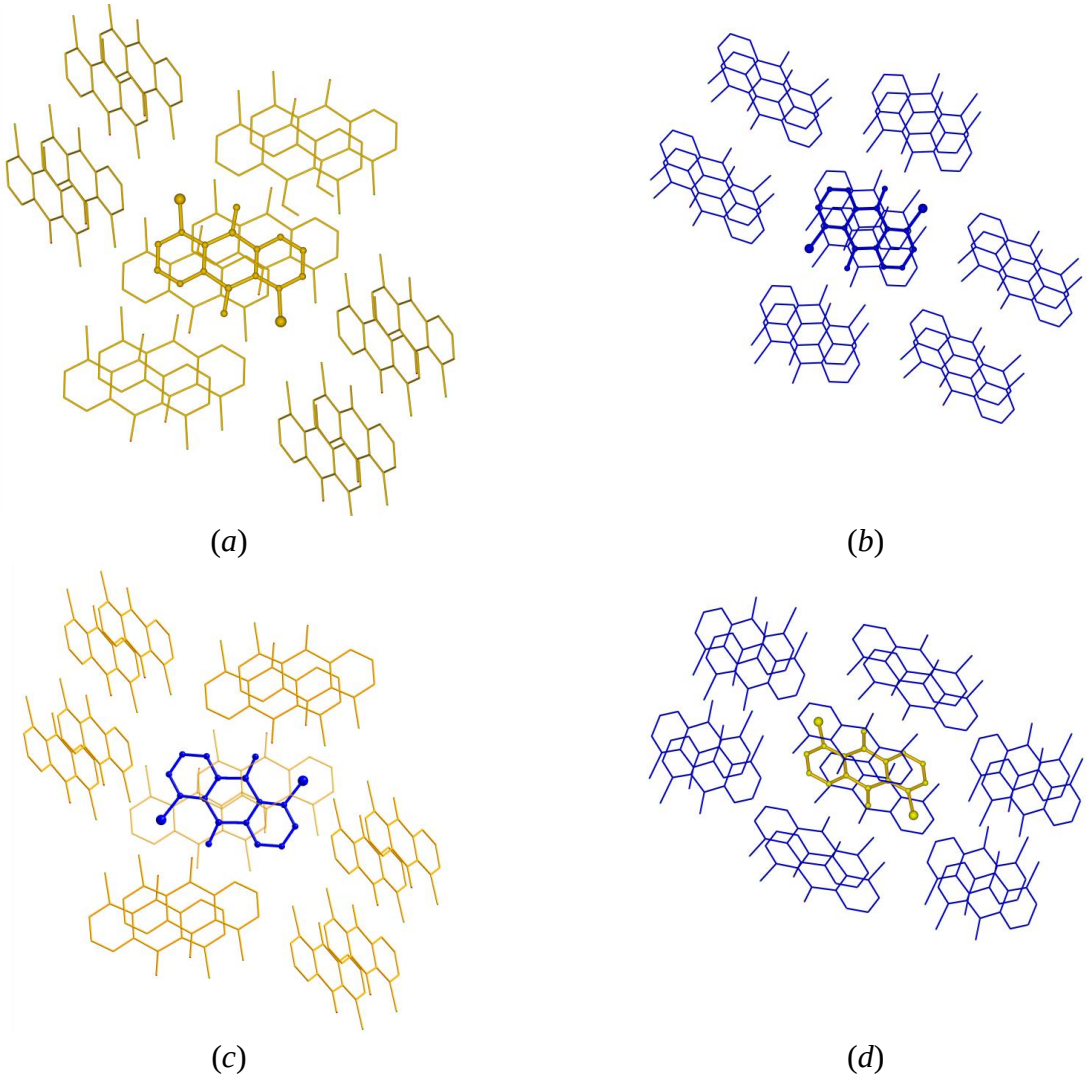

(*a*) (*b*)

(*c*) (*d*)

Figure S6. Molecular clusters built by molecules (III) – central molecule (*a*, *d*) (III)-A, (*b*, *c*) (III)-B**,** surrounding (*a*, *c*) (III)-A, (*b*, *d*) (III)-B. Each central molecule is surrounded by 14 molecules. H atoms are omitted for clarity.

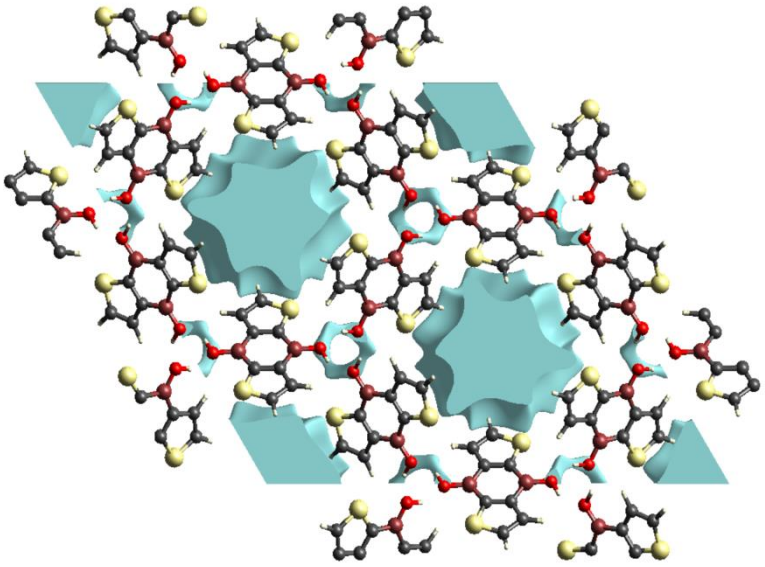

Figure S7. Unit-cell packing diagram for (V) with 0.0003 au. void surface generated in *CrystalExplorer* (Turner *et al.*, 2011).

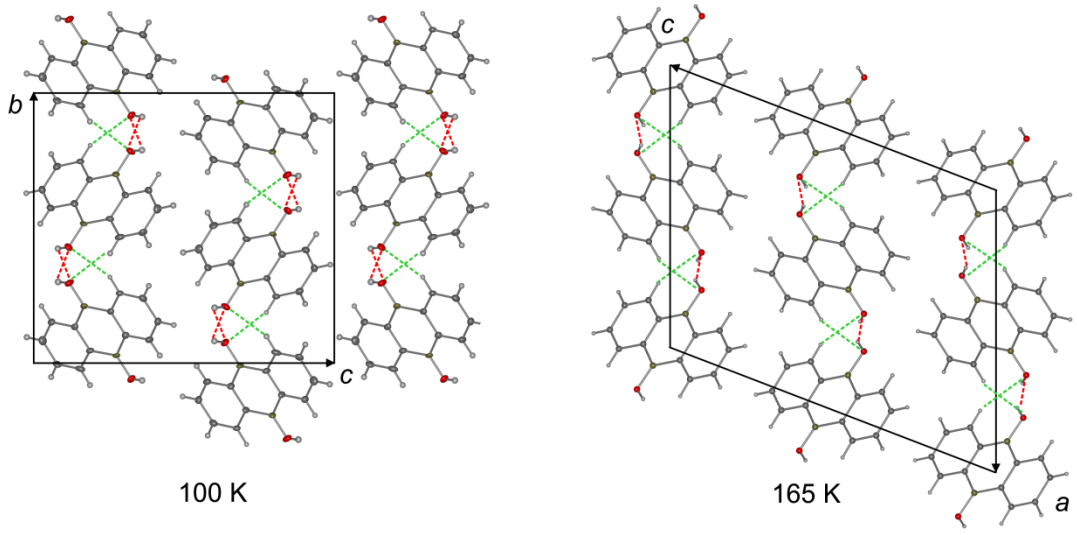

Figure S8. Crystal structure views showing the differences in the layered arrangements in two polymorphic forms of (I).

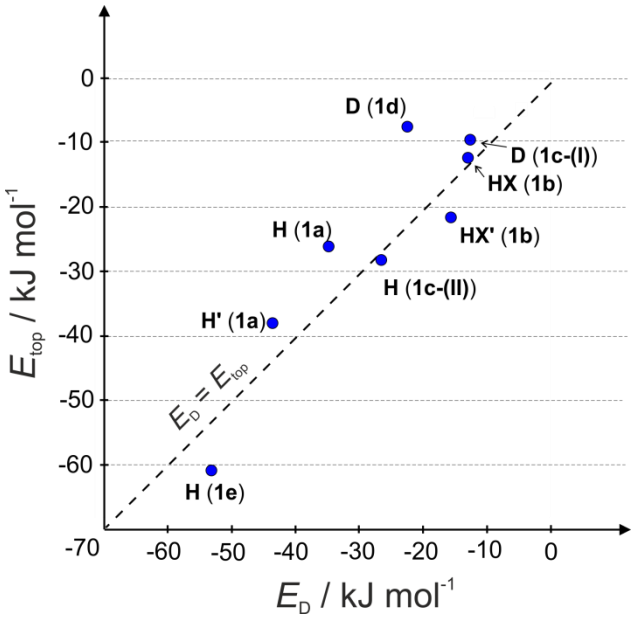

Figure S9. Correlation plot of E_{top} (sum of the interaction energies obtained *via* the Espinosa-Lecomte approach) vs E_D (*PIXEL*-computed dimer interaction energy).

Table S1. Comparison between cohesive energies calculated in *PIXEL* with the X-ray crystal geometries ($E_{coh}^{X\text{-}ray}$, after X-H bonds standardization) and geometries optimized with *CRYSTAL09* (E_{coh}^{opt}). The energy values obtained from *CRYSTAL09* are given in parentheses. Lattice energies breakdown into the electrostatic (E_{elstat}), polarization (E_{pol}), dispersion (E_{disp}) and repulsion (E_{rep}) terms is shown for the optimized geometries.

	(I)	**(II)**	**(III)-A**	**(III)-B**	**(IV)**	**(V)**
$E_{coh}^{X\text{-}ray}$ / kJ·mol^{-1}	-106.1	-115.2	-101.4	-94.0	-113.9	-122.4
E_{coh}^{opt} / kJ·mol^{-1}	-129.5 (-133.5)	-123.3 (-120.3)	-104.9 (-106.0)	-101.8 (-103.7)	-122.7 (-118.6)	-133.4 (-128.8)
E_{elstat} / kJ·mol^{-1}	-119.9	-60.1	-56.2	-62.8	-62.9	-148.0
E_{disp} / kJ·mol^{-1}	-152.8	-131.8	-162.0	-162.5	-173.6	-136.6
E_{pol} / kJ·mol^{-1}	-44.8	-19.6	-23.1	-20.0	-19.2	-79.7
E_{rep} / kJ·mol^{-1}	131.4	91.2	92.7	87.6	97.8	230.8